Modeling fiber flocculation in turbulent flow: a numerical study

Morten Steen

Post-graduate student, *The Norwegian Pulp and Paper Research Institute, Box 115 Vinderen, 0319 Oslo 3, Norway

ABSTRACT *A numerical model for the flocculation process in a turbulent fiber suspension can be used to calculate the flocculation intensity. The model includes the rate of both rupture and aggregation of fiber flocs.*

Calculations of flocculation intensity in a fully developed pipe flow are presented at two different Reynolds numbers (Re). The results show higher flocculation intensity in the center of the pipe than in the wall region. Flocculation intensity in the center of the pipe is greater at the lower Re.

Flocculation intensity in a pipe with abrupt expansion has also been calculated. The results show first a decrease in flocculation intensity at the pipe axis, followed by an increase. Minimum flocculation intensity is predicted at a certain distance downstream of the step, which is close to observations reported in the related literature.

For both geometries, radial mean and turbulent velocity profiles have been compared with measured results in single-phase flow.

KEYWORDS
Analysis
Fibers
Flocculation
Fluid flow
Mathematical analysis
Turbulent flow

Dispersion of fiber flocs by turbulent forces is an important part of the papermaking process and is essential in making a sheet with good formation. Several observations of both the state of flocculation and the flocculation process have been made, and extensive reviews have been presented (*1-4*). However, information is scarce about quantitative models for predicting the state of fiber flocculation in flowing suspensions. The purpose here is to present a numerical model for the mechanical flocculation process in fiber suspensions, a model that can be used to calculate the flocculation intensity.

Background

Anderson (*5*) published a model in which the probability of the rupture of fiber flocs was equal to the product of (a) the probability that a certain fluid stress would occur and (b) the probability that the strength of the floc was lower than this stress. Results from experiments indicated agreement with this model.

Empirical models for both formation and destruction of fiber flocs have been presented by Takeuchi *et al.* (*6*). The models calculated the degree of flocculation, $\Delta c/\bar{c}$, as a function of time after a change has appeared in the pipe flow geometry. The key variables in the models were the wall shear stress and the fiber network plug radius in the core of the pipe. The equations were fitted to data for both softwood and hardwood bleached fibers.

Wagle *et al.* (*7*) stated that the floc breakup process in a steady shear field started as a global deformation and fragmentation at large scale, depending mostly on the shear rate. It was followed by a local small-scale erosion process, for which the floc size reduction was modeled as an exponential rate process in which the rate constant was a function of the shear stress. They indicated that a similar approach could be used to model the global phenomena, however, at a different time scale.

Hourani has published a model for calculating the size distribution of fiber flocs using the mass-action law in combination with the turbulent energy spectrum for two-phase flow (*8, 9*). He assumed that a "dynamic equilibrium" existed between fibers and flocs and that the mean floc scale was equal to the mean turbulent eddy size. The model results agreed well

*Steen is now engineer of product development, Inenco A/S, Gjerdrumsvei 10A, N-0486 Oslo 4, Norway.

Nomenclature

- A = rate of floc aggregation
- Δc = consistency fluctuation
- c = fiber consistency
- c' = fluctuation in consistency
- c^{λ} = consistency in fine structure regions
- D = pipe diameter
- d = fiber diameter
- E = modulus of elasticity
- $1/EI$ = fiber flexibility
- I = moment of inertia
- k = turbulent kinetic energy
- L = length of pipe
- l = fiber length
- l' = turbulent length scale
- l^* = turbulent length scale in fine structure
- m = mass
- p = pressure
- R = rate of floc rupture
- r = distance in radial direction
- Re = Reynolds number, Re = u D/ν
- t' = turbulent time scale
- t_{fiber} = fiber response time
- u = axial velocity
- u' = fluctuating axial velocity
- u^* = turbulent velocity in fine structure
- x = distance in axial direction
- y = distance from wall
- $y+$ = nondimensional distance from wall
- v = radial velocity

Greek symbols

- α = viscous damping coefficient
- β = damping factor = $a/(m\omega_0)$
- $\Gamma\phi$ = transport coefficient
- $\gamma\lambda$ = fraction of fine structure regions
- ϵ = turbulent dissipation
- κ = von Karman constant
- μ = dynamic viscosity
- μ_t = turbulent viscosity
- ν = kinematic viscosity
- ρ = density of fluid
- σ_{Φ} = Prandtl-Schmith number
- τ = shear stress
- ω = frequency for turbulent fine structure
- ω_0 = eigen frequency for fibers
- Φ = dependent variable

Superscripts

- λ = fine structure regions
- $*$ = fine structure
- $-$ = mean quantities
- $'$ = fluctuating quantities

Subscripts

- in = inlet condition
- out = outlet condition
- b = bulk
- cl = centerline
- eff = effective
- R = reattachment

1. Mean axial velocity profile in a fully developed pipe flow. (*Re* = 50,000, data from Laufer (*21*))

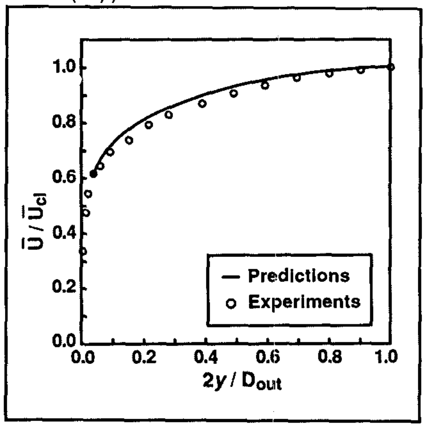

2. Turbulent kinetic energy profile in fully developed pipe flow. (*Re* = 50,000, data from Laufer (*21*))

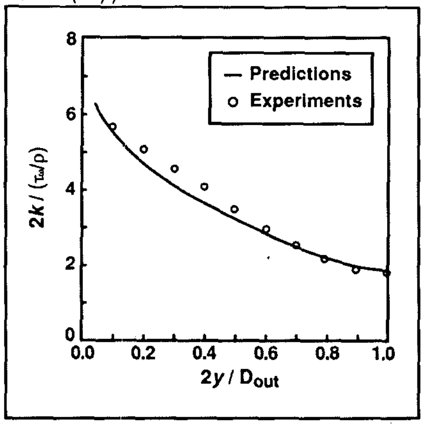

3. Production and dissipation profiles of turbulent kinetic energy in fully developed pipe flow. (*Re* = 50,000, data from Laufer (*21*))

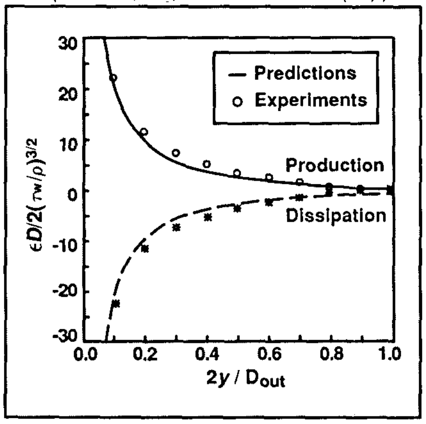

with measured results of floc size distributions for both softwood and hardwood fibers.

The turbulent shear stress is an important variable in the floc dispersion process. Numerical predictions of turbulent flow fields are therefore of interest when designing process equipment for the paper industry. Ten years ago, Baliaga and Majumdar (*10*) presented an extensive review of available numerical methods. However, few publications have appeared in this field in the pulp and paper literature because it is difficult to model the effects the fibers have on the turbulent structure and because of the lack of complete models for the fiber flocculation process.

Li and Majumdar (*11*) presented the governing equations for single-phase flow, including the k-ϵ model for turbulence. The turbulent flow field in a channel with an asymmetric sudden expansion was calculated, and the profiles of mean and fluctuating velocity were in fair agreement with measurements. They claimed that the model should be valid for the general hydraulic characteristics of low-consistency fiber suspensions.

Full three-dimensional calculations of a tapered manifold flow spreader were presented by Syrjälä *et al.* (*12*) using the same flow equations as Li and Majumdar (*11*). Their predictions of axial velocities at various axial positions downstream agreed well with measurements. Jones and Ginnow (*13*) have published calculations of turbulence intensity in decaying turbulence downstream of a grid, with the results in close agreement with experimental results. However, their predictions of average velocity at various axial positions in a tapered headbox compared poorly with measured velocities. The turbulent flow field in a circular step diffusor has been calculated by Lin (*14*) using the Prandtl's mixing theory with a specified length scale. (A circular step diffusor is the same as an abrupt pipe expansion.) The predictions were not compared with experimental data.

More general quantitative models for describing the fiber flocculation process are needed for the design of equipment in the papermaking process. For the purpose of meeting this challenge, a fiber flocculation concept was implemented in a numerical flow model (*15*). With this model, based on the turbulent flow variables, the flocculation intensity, $\overline{c'^2}/\bar{c}^2$, has been calculated for an equilibrium flow, as in a circular pipe flow, and for a nonequilibrium flow, as in a circular step diffusor. The latter geometry is encountered in the papermaking process. This geometry was also a crucial test of the fiber flocculation concept, showing a decrease in flocculation intensity followed by an increase.

Mathematical models

Governing equations for turbulent fluid flow

In modeling fluid flow in an axisymmetric pipe, the geometry can be represented in two dimensions by using cylindrical coordinates. The governing equations (*16*) for stationary flow can be written as follows.

Continuity equation:

See Equation 1

Momentum equations. Axial x-direction:

See Equation 2

Radial r-direction:

See Equation 3

The turbulent viscosity, μ_t, is calculated from a k-ϵ turbulence model:

See Equations 4 and 5

Turbulent kinetic energy equation:

See Equations 6 and 7

Turbulent energy dissipation equation:

See Equation 8

The constants in the model are: $C_D = 0.09$, $C_1 = 1.44$, $C_2 = 1.92$, $\sigma_k = 1.0$, and $\sigma_\epsilon = 1.3$.

The boundary conditions at the pipe axis and in the outlet are all zero-gradient conditions, $\delta\Phi/\delta x_j = 0$, for all variables. In the inlet, we have either used measured profiles or 1/7 power velocity profiles. Then, k and ϵ are calculated by setting the production of turbulent kinetic energy equal to the dissipation of turbulent kinetic energy. At solid boundaries, the velocities are zero. To avoid an extremely fine grid resolution near the walls, we use a "law of the wall" (*17*) for calculating τ_w, and k, and ϵ in the control volume near the wall.

Shear stress at the wall:

See Equation 9

Dissipation in the k equation:

See Equation 10

Dissipation in mode adjacent to the wall:

See Equation 11

All the governing equations are of the same type:

See Equation 12

These equations were solved by using the KAMELON numerical flow code (*18*). This is a general finite difference program in which the equations are integrated over control volumes and the pressure is solved by the SIMPLE algorithm of Patankar (*19*). The resulting set of coupled algebraic equations are solved by TDMA (tri-diagonal matrix algorithm). Using a grid with 60 × 30 nodes, 450 iterations gave a convergent solution for the abrupt pipe expansion, which, incidentally, demanded 4 h of CPU time on a VAX-station 3100.

Fiber flocculation concept

As mentioned, a concept for fiber flocculation in turbulent flow has been presented (*15*). Both the floc rupture and aggregation mechanisms in the fiber flocculation process were discussed in detail, based on results from experiments and data from related literature. Hence, only a condensed review of the concept is presented here, together with the mathematical models for calculating flocculation intensity.

In turbulent fiber suspensions, the large eddies will contain local fiber networks, or flocs, while the smallest vortices will contain only single fibers or no fibers at all. During the turbulent energy transfer from larger to smaller scales by vortex stretching (the turbulent energy cascade), the internal fiber network is deformed. Floc breakup is probable if the deformation forces are larger than the flocs' internal network strength. The length scale of the straining vortices will be of the same order as the floc scale. Eddies of a smaller scale will agitate the outer part of the floc, making the floc weaker and making rupture more likely.

Flocs of one length scale can be transported by turbulent eddies of larger scale, and floc collisions will occur. Turbulent eddies of small length scale will "activate" the outer part of the floc and single free fibers by bending and vibrating simple fibers. The turbulent fine structures located between larger eddies play a dominant role in this process. Collisions of flocs cause buildup when the contact time is long enough for the newly formed local floc network to settle. Finally, we will have local small-scale erosion and deposition of single fibers on the surfaces of flocs.

In the fiber flocculation concept, the rupture of flocs is linked to the turbulent energy cascade, whereby eddies interact with other eddies of adjacent length scale. However, the floc aggregation process is composed of a small-scale activation and a large-scale collision and network settling. Fortunately, both subprocesses take place at the same location but at different times, since the activating turbulent fine structures are located between the large turbulent eddies. [Details on the structure of turbulence can be found in Magnussen (*20*).]

4. Mean axial velocity profiles at various axial positions in a circular step diffusor. (*Re* = 72,000, data from Ha Mihn and Chassaing (*22*))

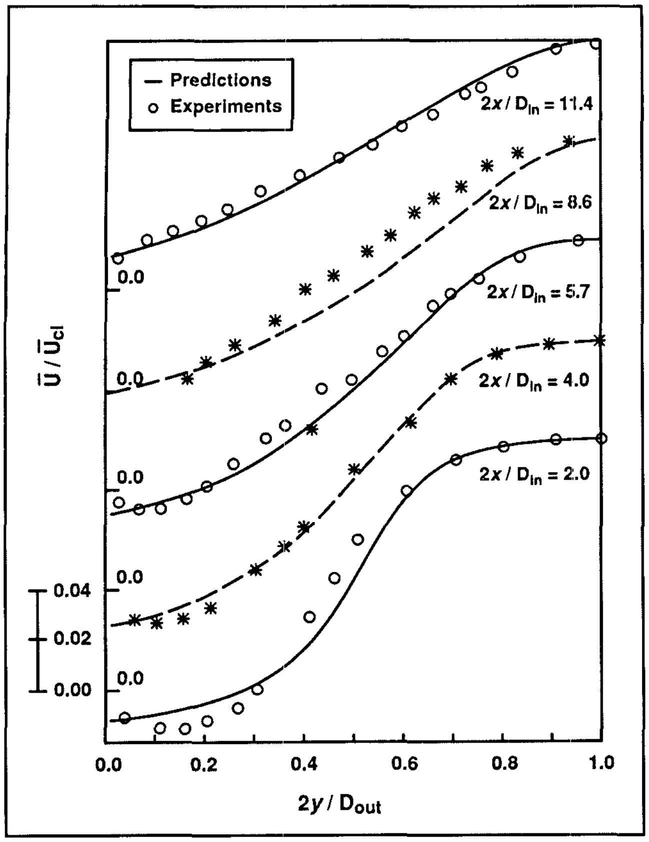

5. Turbulent kinetic energy profiles at various axial positions in a circular step diffusor. (*Re* in = 72,000, data from Ha Mihn and Chassaing (*22*))

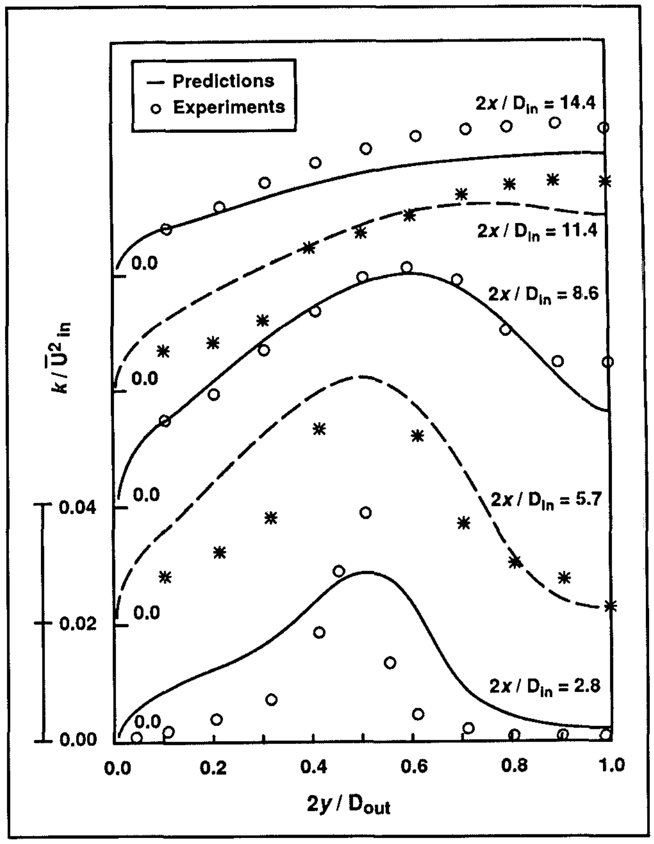

The conservation of flocculation intensity is modeled by a standard transport equation (*10*), setting $\Phi = \overline{c'^2}/\bar{c}^2$. The source term includes terms for both the rate of floc aggregation and rupture.

See Equation 13

The turbulent energy transfer down to smaller length scale is described by ϵ in the k-ϵ model, and we may model the rate of floc rupture as:

See Equation 14

The aggregation of flocs is initiated at the interface between existing flocs and the activating regions. Let us assume that the fine structure regions cause the fiber activation and that the rate of floc formation depends on the concentration within this region and in the floc itself.

See Equation 15

The rate of fiber activation is proportional to the mass transfer to the turbulent fine structures (u^*/l^*) and the fine structures' energy efficiency in activating single fibers. Assuming the energy efficiency can be modeled by the resonance energy transfer coefficient, $f(\phi/\phi_0)$, in a forced and damped oscillating system, we then have Eq. 16.

See Equation 16

The rate of fiber floc formation depends also on the flocs' contact time and the fiber response time. Hence: the total rate of aggregation will then be:

See Equation 17

See Equation 18

Results

Single-phase flow

To verify the turbulent flow field, single-phase calculations of a fully developed pipe flow and a flow in an abrupt pipe expansion (circular step diffusor) were compared with data from the related literature.

Predicted results from a fully developed pipe flow were compared with data from Laufer (*21*) at Re = 50,000. **Figure 1** displays the mean velocity

6. Flocculation intensity profiles in turbulent fully developed pipe flow

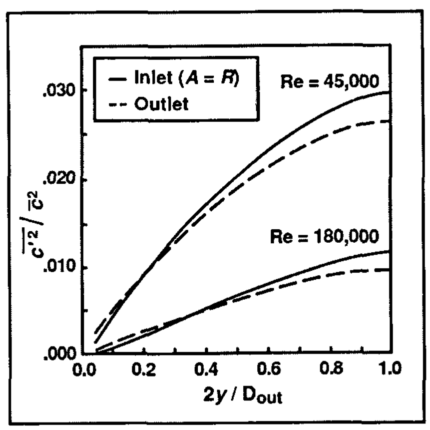

profile, and **Fig. 2** shows the turbulent kinetic energy profile. Production and dissipation of turbulent kinetic energy are plotted in **Fig. 3**. The predictions agree very well with the results measured.

Results for an abrupt pipe expansion (D_{out}/D_{in} = 2, where the diameter becomes twice as large) at Re_{in} = 72,000 were compared with measured data from Ha Mihn and Chassaing

7. Flocculation intensity profiles at various axial positions in a circular step diffusor

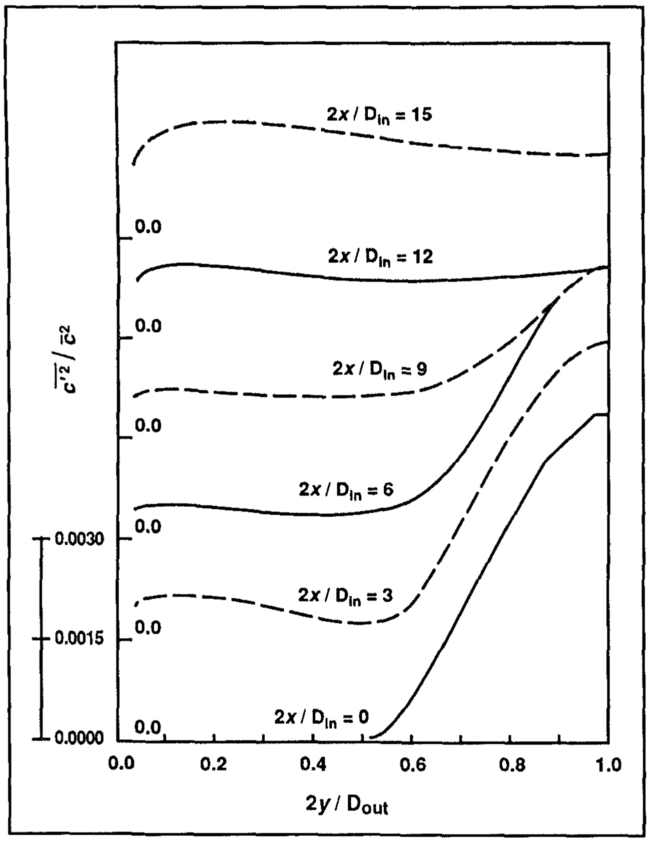

9. Measured flocculation intensity profiles at various axial positions downstream of a small step (D_{in}/D_{out} = 0.8) in pipe flow

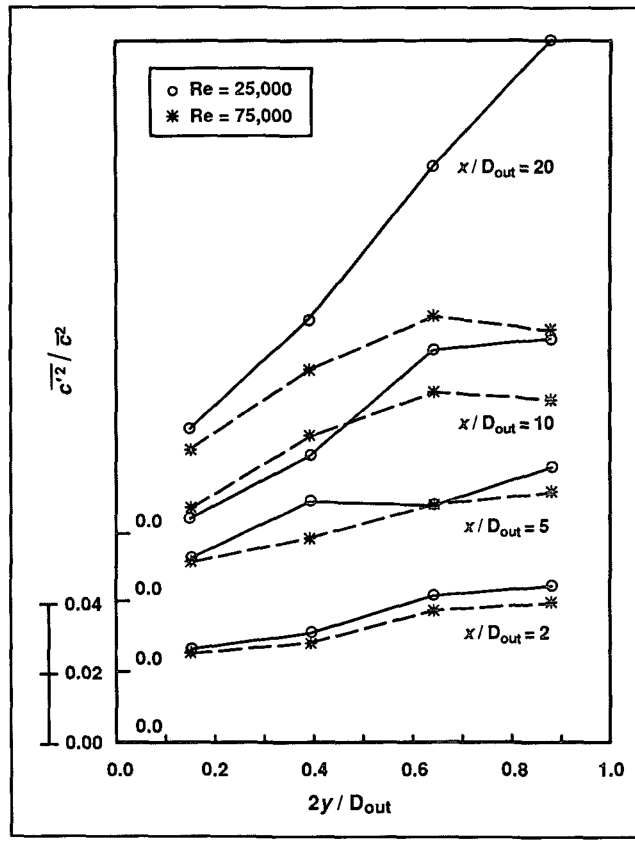

8. Flocculation intensity at various axial positions for two radial positions in a circular step diffusor

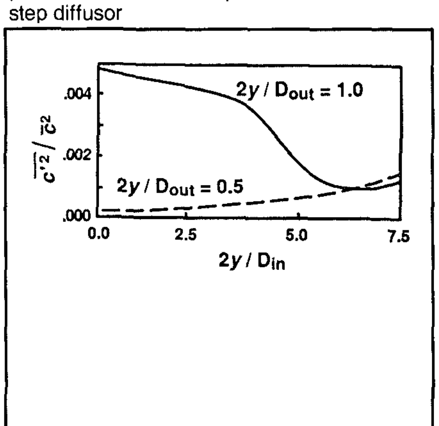

(*22*). **Figure 4** shows the mean axial velocity profiles, and **Fig. 5** displays the turbulent kinetic energy profiles at various positions downstream of the step.

The reattachment length is of the right order ($2X_R/D_{in}$ = 8.6), even if there are several discrepancies between the predictions and the measured data. The turbulent kinetic energy is too high in the recirculation zone, causing turbulent shear stress and momentum transfer to be too high. This is a weakness of the k–ϵ model, which predicts too large a turbulent length scale in the recirculating region (*23*). The predictions of Ha Mihn and Chassaing fit their measured data better than our model does, but their results were obtained with slightly altered constants in the turbulence model.

A different constant in the equation was also used by Moon and Rudinger (*24*). That constant gave a correct reattachment length, but the decay of the centerline mean velocity was then incorrectly predicted. The mean velocity profiles of Moon and Rudinger (*24*) and Lin (*14*) seem to suffer from the same weakness, in the near wall region, as our predictions.

Flocculation

We have calculated flocculation intensity in an axisymmetric, fully developed pipe flow with diameter D_{out} = $2D_{in}$ = 0.05 m and length $L = 7.5D_{in}$ = 0.1875 m. A fiber suspension with $\bar{c}$ = 0.005, l = 3 mm, d = 30 μm, and $EI = 10^{-12}$ N·m² was simulated. The model has not been calibrated, and we assume that the turbulent structure is unchanged in the presence of the fibers. This assumption should be studied critically when more data are available on turbulence and flocculation intensity. Hence, $\sigma_{\overline{c'^2}/\bar{c}^2} = C_{f1} = C_{f2} = 1$.

The time response for fibers, t_{fiber}, and the damping factor, β, are both related to the eigen frequency of the fibers and the viscosity of the fluid. The viscous damping coefficient, α, can be calculated from the drag on a thin circular cylinder. In this introductory approach, we have set β = 10 and t_{fiber} = 1, indicating a strong nonperiodic damping of the fiber oscillations.

Figure 6 shows profiles of $\overline{c'^2}/\bar{c}^2$ at two different Reynolds numbers, Re = 45,000 and 180,000 (u_{cl} = 1 m/s and 4 m/s). Both the inlet profiles based on $A = R$ and the calculated outlet profiles are presented. In an equilibrium flow, these profiles are similar in shape. The flocculation intensity in the wall region is lower than in the center, and the intensity increases with decreasing Reynolds number.

A circular step diffusor with the same pipe geometry as described above has also been calculated. The diameter in the inlet is $D_{in} = D_{out}/2$ and $Re_{in} = 90{,}000$ ($u_{cl} = 4$ m/s). The radial flocculation intensity profiles at various downstream positions are presented in **Fig. 7**. The inlet profile is based on $A = R$, and further downstream we observe how the flocculation intensity at the pipe axis decreases. Far downstream of the step, it increases again with minimum flocculation intensity at $x/D_{in} = 6.5$, as shown in **Fig. 8**. The flocculation intensity in the inlet for $u_{cl} = 4$ m/s is lower in Fig. 7 than in Fig. 6 as a result of a smaller turbulent length scale.

Discussion

Few reports in the related literature can be used in a discussion of these results. However, it is still pertinent to discuss the formulation of the model, some of the results of our own measurements, and observations from the literature.

Rupture and aggregation model

The rupture term (R in Eq. 14, signifying the dissipation of the fluctuation) is similar to the one used by Rodi (*25*) in the governing equation for a general scalar fluctuation. Rearranging Eq. 14, we obtain Eq. 19.

See Equation 19

The decay of a fluctuation is proportional to the decay of turbulent energy, and $1/C_{f2}$ should be between 0.5 and 1 (*25*). Equation 19 is also a ratio of two time scales or two frequency scales. A value of $1/C_{fs}$ equal to 1 indicates that the break-up of flocs takes place when the frequency of the turbulent eddies is resonant with some eigen frequency of the flocs.

The aggregation term (A) is different from the production term used by Rodi (*25*). The production of a scalar fluctuation is controlled by mean scalar gradients, while floc aggregation starts out as a small-scale activation of fibers followed by floc collisions and fiber network settling. The flocculation process is a two-way hierarchy and not a one-way process, as is the decay of a scalar fluctuation (*15*).

The interaction between the small-scale activation and large-scale collisions is essential for modeling the floc buildup. The small-scale activation takes place in the turbulent fine-structure regions, which are only a small fraction of the total flow volume (*20*). The regions of fine structure are located close to the large-scale eddies. Equation 15 can be seen as an analogy to the kinetic reaction rate in chemical reactions, including the fiber consistency inside flocs and the fiber consistency in the activating regions. In the model, we have proposed expressions for these two consistencies.

The ability of fibers to bend depends on the fiber flexibility and fiber length. Within the regions of fine structure, we will find the turbulent fine structures as vortex tubes. The vortex tube is generated at the rate of the mass transfer, u^*/l^*, to the turbulent fine structure (*20*). The rate of energy transfer from turbulent eddies to fiber oscillations is at a maximum when the frequency of fine structures equals the eigen frequency of the fibers ($\omega/\omega_0 = 1$).

When we do not have a resonant system, the rate of energy transfer can be expressed by a coefficient, $f(\omega/\omega_0)$. It is easier to activate a long and flexible fiber than a short and stiff one, causing a greater aggregation term. Furthermore, if the frequency of the turbulent fine structures, u^*/l^*, becomes lower, the fibers will not be activated to the same degree, causing a smaller aggregation term. This finding matches observations by Steenberg *et al.* (*26*) when the viscosity of the fiber suspension was increased ($u^*/l^* \approx 1/\nu$). Their explanation was that an increase in viscosity increased the time for the fibers to come to rest after activation. We denote this time as t_{fiber}, and the floc buildup rate is proportional to the ratio t'/t_{fiber}.

Comparisons with data from experiments

On the basis of the technique published earlier (*15*), flocculation intensity has been calculated from still photos of a fiber suspension in a pipe flow taken in transmitted flash light. With image analysis and Fast Fourier Transform, flocculation spectra were recorded at various radial regions across the pipe. These spectra were later integrated to give the total flocculation intensity.

A vertical pipe flow of softwood fibers with consistency $\bar{c} = 0.0017$ was studied, and photos were taken at various positions (x/D_{out}) downstream of an orifice ($D_{in}/D_{out} = 0.8$, $D_{out} = 23.8$ mm). The results for two different Reynolds numbers, $Re = 25{,}000$ and $75{,}000$ ($u_b = 1$ and 3 m/s) are presented in **Fig. 9**. Even though the geometry, Reynolds number, and fiber concentration are different from our calculations, the results can still be used for a discussion of the presented predictions.

The flocculation intensity in the center of the pipe is higher at the lower flow rate, and the difference in flocculation intensity between $Re = 25{,}000$ and $Re = 75{,}000$ is increasing downstream. At $x/D_{out} = 20$, we observe a higher flocculation intensity in the center of the pipe for $Re = 25{,}000$ than for $Re = 75{,}000$. The flocculation intensity in the wall region is lower than in the center. The same effects can be observed in our predictions of the fully developed flow in Fig. 6.

Near the orifice, one can observe a flat flocculation intensity profile ($x/D_{out} = 2$). In our predictions of the circular step diffusor (Figs. 7 and 8), the flocculation intensity in the center decreases downstream of the step before it increases again after $x/D_{in} = 6.5$. At this point, the profile is very flat, and the position corresponds to $x/D_{out} = 3.25$. Hence, our predictions of both the equilibrium and the non-equilibrium flow show analogies to recorded data.

Observations from related literature

d'Incau found (*27*), in a decaying flow field downstream of a grid, that a minimum in flocculation intensity corresponded to a maximum in turbulent strain rate (u'/l'). In our model, we have set the rupture term (R in Eq. 14) proportional to u'/l'. d'Incau measured his maximum turbulent strain rate at $x/D_{in} = 7$, and we have minimum flocculation intensity in the center of the pipe at $x/D_{in} = 6.5$. Knowing the large difference between the flow field in a step diffusor and a flow field downstream of a grid, we were able to make predictions that compare well with d'Incau's observations.

A study of the scale of flocculation in fully developed turbulent pipe flow has been carried out by Persinger (*28*). His measurements show that the floc length scale, l_{floc}, decreases with increasing Reynolds number, and the length scale is larger in the center of the pipe than in the wall region. The scale of floc length could be predicted from setting $A = R$, which in the fully developed pipe flow would give $l_{floc} = l'$. The term l_{floc} is then smaller in the wall region than in the center, but l' does not change with Reynolds number. Hence, this result would not fit the results of Persinger (*28*).

The model presented here is an introductory approach to the calculation of flocculation intensity and the length scale in turbulent fiber suspensions. Although the model gives reasonable results, more complex effects should be studied and implemented in it. One aspect that should be included is the effect the fibers have on the turbulent structure, which corresponds to Hourani's calculations of floc size distribution (*8, 9*). Data reported earlier (*29*) and a two-phase k-ϵ model (*30*) both indicate reduced turbulent kinetic energy in the presence of fibers and particles. Furthermore, the effect of the concentration gradient in a flowing fiber suspension has been omitted in this study. Finally, there should be a calculation of a floc length scale that corresponds to an equilibrium scale for which the rate of floc aggregation equals the rate of rupture.

Conclusions

Flocculation intensity in a turbulent fiber suspension can be calculated by using a transport equation for $\overline{c'^2}/\bar{c}^2$. The model includes source terms for both the rate of floc rupture and aggregation. The rate of floc rupture is proportional to the turbulent strain rate. The floc aggregation rate is proportional to consistency within the floc itself and the consistency in the surrounding activating regions.

The model has been used to calculate $\overline{c'^2}/\bar{c}^2$, in a fully developed axisymmetric pipe flow at two different Reynolds numbers. $\overline{c'^2}/\bar{c}^2$ at the pipe axis is lower for $Re = 180{,}000$ than for $Re = 45{,}000$. In the wall region, the $\overline{c'^2}/\bar{c}^2$ is lower than in the center of the pipe.

Flocculation intensity in a circular step diffusor with $D_{out}/D_{in} = 2$ has been calculated. Starting with fully developed flow conditions in the inlet and $Re = 90{,}000$, the model predicts a decrease in $\overline{c'^2}/\bar{c}^2_{cl}$, with a minimum at $x/D_{in} = 6.5$. Further downstream, the flocculation intensity in the center of the pipe increases again.□

Literature cited

1. Parker, J. D., The Sheet Forming Process, TAPPI STAP No. 9, Atlanta, 1972.
2. Norman, B. G., Moller, K., Ek, R., and Duffy, G. G., The 6th Fundamental Research Symposium, British Paper and Board Ind. Fed., Technical Div., London, 1978, p. 195.
3. Kerekes, R. J., Soszynski, R. M., and Tam Doo, P. A., The 8th Fundamental Research Symposium, Mechanical Engineering Publications, Ltd., London, 1985, p. 265.
4. Soszynski, R. M., Ph.D. thesis, University of British Columbia, Vancouver, Canada, 1987.
5. Anderson, O., Svensk Papperstid. 69(2): 23(1966).
6. Takeuchi, N., Senda, S., Namba, K., and Kuwabara, G., APPITA, 37(3): 223(1983).
7. Wagle, D. G., Lee, C. W., and Brodkey, R. S., 1987 Engineering Conference Proceedings, TAPPI PRESS, Atlanta, p. 447.
8. Hourani, M. J., Tappi J. 71(5): 115(1988).
9. Hourani, M. J., Tappi J. 71(6): 186(1988).
10. Baliaga, B. R. and Majumdar, A. S., Intl. Symposium on Paper Machine Headboxes, McGill University, Montreal, Canada, 1979, p. 74.
11. Li, Y-K. and Majumdar, A. S., Intl. Symposium on Paper Machine Headboxes, McGill University, Montreal, Canada, 1979, p. 64.
12. Syrjälä, S., Saarenrinne, P., and Karvinen, R., 1988 Engineering Conference Proceedings, TAPPI PRESS, Atlanta, p. 233.
13. Jones, G. L. and Ginnow, R. J., 1988 Engineering Conference Proceedings, TAPPI PRESS, Atlanta, p. 15.
14. Lin, J. Y., 1988 Engineering Conference Proceedings, TAPPI PRESS, Atlanta, p. 21.
15. Steen, M., The 9th Fundamental Research Symposium, Mechanical Engineering Publications Ltd., London, 1989, p. 251.
16. Gosman, A. D., Khalil, E. E., and Whitelaw, J. H., Turbulent Shear Flows I, selected papers from 1st Intl. Symposium on Turbulent Shear Flows, Springer Verlag, Heidelberg, 1979, p. 237.
17. Laudner, B. E. and Spalding, D. B., Computer Methods in Applied Mechanics and Engineering, Vol. 3, North-Holland Publishing Comp., 1974, p. 269.
18. Berge, G., Østby, O., and Magnussen, B. F., KAMELON, a description of the numerical method and the solution procedure. The Norwegian Institute of Technology, Trondheim, January 1987.
19. Patankar, S. V., Numerical Heat Transfer and Fluid Flow, McGraw-Hill, New York, 1980.
20. Magnussen, B. F., 19th Aerospace Science Meeting, American Inst. of Aeronautics and Aerospace, Washington, D.C., 1981.
21. Laufer, J., The structure of turbulence in fully developed pipe flow, U.S. NACA Tech. Report 1174, 1954.
22. Ha Mihn, H. and Chassaing, P., Turbulent Shear Flows I, selected papers from 1st Intl. Symposium on Turbulent Shear Flows, Springer Verlag, Heidelberg, 1979, p. 178.
23. Laudner, B. E., Turbulence models and their application, Vol. 2, Editions Eyrolles, Paris, 1984, p. 5.
24. Moon, L. F. and Rudinger, G., J. of Fluids Eng., Trans. of ASME (March): 226(1977).
25. Rodi, W., Turbulence Models and their Application in Hydraulics, 2nd edn., Intl. Assoc. for Hydraulic Research, Delft, 1984.
26. Steenberg, B., Thalen, N., and Wahren, D., The 3rd Fundamental Research Symposium, British Paper and Board Makers Assoc., Technical Section, London, 1966, p. 177.
27. d'Incau, S., 1983 Engineering Conference Proceedings, TAPPI PRESS, Atlanta, p. 583.
28. Persinger, W. H. and Meyer, H., Papper och Trä 57(9): 563(1975).
29. Steen, M., Nordic Pulp Paper Res. J. 4(4): 244(1989).
30. Elgobashi, S. E. and Abou-Arab, T. W., Phys. of Fluids 26(4): 931(1983).

The author thanks Bjørn F. Magnussen for valuable contributions during discussions of the fiber flocculation model. Simon Papworth is acknowledged for his linguistic revision of the manuscript. This study was done as a part of a Ph.D. thesis at The Norwegian Institute of Technology with financial support from The Royal Norwegian Council for Scientific and Industrial Research.

Received for review June 5, 1990.

Accepted Dec. 30, 1990.

Presented at the TAPPI 1990 Engineering Conference.

Please see equations, next page.

Equations

$$\frac{\partial}{\partial x}(\rho u) + \frac{1}{r}\frac{\partial}{\partial r}(\rho r v) = 0 \tag{1}$$

$$\frac{\partial}{\partial x}(\rho u^2) + \frac{1}{r}\frac{\partial}{\partial r}(\rho r u v) = -\frac{\partial p}{\partial x} + 2\frac{\partial}{\partial x}\left(\mu_{\text{eff}}\frac{\partial u}{\partial x}\right) + \frac{1}{r}\frac{\partial}{\partial r}\left(\mu_{\text{eff}} r\frac{\partial u}{\partial r}\right) + \frac{1}{r}\frac{\partial}{\partial r}\left(\mu_{\text{eff}} r\frac{\partial v}{\partial x}\right) \tag{2}$$

$$\frac{\partial}{\partial x}(\rho u v) + \frac{1}{r}\frac{\partial}{\partial r}(\rho r v^2) = -\frac{\partial p}{\partial r} + \frac{\partial}{\partial x}\left(\mu_{\text{eff}}\frac{\partial v}{\partial x}\right) + 2\frac{1}{r}\frac{\partial}{\partial r}\left(\mu_{\text{eff}} r\frac{\partial v}{\partial r}\right) + \frac{\partial}{\partial x}\left(\mu_{\text{eff}}\frac{\partial u}{\partial r}\right) - 2\mu_{\text{eff}}\frac{v}{r^2} \tag{3}$$

$$\mu_t = C_{D\rho}\frac{k^2}{\epsilon} = C_D^{1/4}\rho k^{1/2} l' \tag{4}$$

$$\mu_{\text{eff}} = \mu + \mu_t \tag{5}$$

$$\frac{\partial}{\partial x}(\rho u k) + \frac{1}{r}\frac{\partial}{\partial r}(\rho r v k) = \frac{\partial}{\partial x}\left(\frac{\mu_t}{\sigma_k}\frac{\partial k}{\partial x}\right) + \frac{1}{r}\frac{\partial}{\partial r}\left(\frac{\mu_t}{\sigma_k} r\frac{\partial k}{\partial r}\right) + G_k - \rho\epsilon \tag{6}$$

$$G_k = \mu_t\left\{2\left(\frac{\partial u}{\partial x}\right)^2 + 2\left(\frac{\partial v}{\partial r}\right)^2 + 2\left(\frac{v}{r}\right)^2 + \left(\frac{\partial u}{\partial r} + \frac{\partial v}{\partial x}\right)^2\right\} \tag{7}$$

$$\frac{\partial}{\partial x}(\rho u \epsilon) + \frac{1}{r}\frac{\partial}{\partial r}(\rho r v \epsilon) = \frac{\partial}{\partial x}\left(\frac{\mu_t}{\sigma_\epsilon}\frac{\partial \epsilon}{\partial x}\right) + \frac{1}{r}\frac{\partial}{\partial r}\left(\frac{\mu_t}{\sigma_\epsilon} r\frac{\partial \epsilon}{\partial r}\right) + \frac{\epsilon}{k}(C_1 G_k - C_2\rho\epsilon) \tag{8}$$

$$\frac{u_p}{(\tau_w/\rho)} C_D^{1/4} k_p^{1/2} = \frac{1}{\kappa}\, ln\left(9.0 y_p \frac{C_D^{1/4} k_p^{1/2}}{\nu}\right) \tag{9}$$

$$\int_0^{y_p} \epsilon\, dy = C_D^{3/4}\frac{k_p^{3/2}}{\kappa}\, ln\left(9.0 y_p \frac{C_D^{1/4} k_p^{1/2}}{\nu}\right) \tag{10}$$

$$\epsilon_p = C_D^{3/4}\frac{k_p^{3/2}}{\kappa y_p} \tag{11}$$

$$\frac{\partial}{\partial x}(\rho u \Phi) + \frac{1}{r}\frac{\partial}{\partial r}(\rho r v \Phi) = \frac{\partial}{\partial x}\left(\Gamma_\Phi\frac{\partial \Phi}{\partial x}\right) + \frac{1}{r}\frac{\partial}{\partial r}\left(\Gamma_\Phi r\frac{\partial \Phi}{\partial r}\right) + S_\Phi \tag{12}$$

$$S\ \overline{c'^2}/\overline{c}^2 = \rho(A - R) \tag{13}$$

$$R = C_{f2}\frac{\epsilon}{k}\frac{\overline{c'^2}}{\overline{c}^2} \approx \frac{u'}{l'}\frac{\overline{c'^2}}{\overline{c}^2} \tag{14}$$

$$A \approx (\overline{c} + c')(1 - \gamma^\lambda)c^\lambda\gamma^\lambda \tag{15}$$

$$A \approx \frac{u^*}{l^*} f\left(\frac{w}{w_0}\right) \tag{16}$$

$$A \approx \frac{k}{\epsilon}\frac{1}{t_{fiber}} \approx \frac{t'}{t_{fiber}} \tag{17}$$

$$A = C_{f1}\frac{(\overline{c} + c')(1 - \gamma^\lambda)c^\lambda\gamma^\lambda}{\overline{c^2}}\frac{u^*}{l^*} f\left(\frac{w}{w_0}\right)\frac{k}{\epsilon}\frac{1}{t_{fiber}} \tag{18}$$

$$\begin{aligned}
\gamma^\lambda &= u^*/u' \\
\overline{c} &= (\overline{c} + c')(1 - \gamma^\lambda) = c^\lambda\gamma^\lambda \\
u^* &= 1.74(\nu\epsilon)^{1/4} \\
l^* &= 1.43\,(\nu^3/\epsilon)^{1/4} \\
f(w/w_0) &= (w/w_0)^2/\{[1 - (w/w_0)^2]^2 + \beta^2(w/w_0)^2\} \\
w &= u^*/l^* \\
w_0 &= (4EI/\rho d^2 l^4)^{1/2}
\end{aligned}$$

$$1/C_{f2} = \left(\overline{c'^2}/\overline{c}^2 R\right) / (k/\epsilon) \tag{19}$$